High-Quality Phosphorus-doped MoS_2 Ultrathin Nanosheets with Amendable ORR Catalytic Activity

Hao Huang, Xun Feng, Cuicui Du, and Wenbo Song*

[*] *Hao Huang, Xun Feng, Cuicui Du, and Prof. Wenbo Song*
College of Chemistry, Jilin University, Changchun, 130012, P.R. China
E-mail: wbsong@ jlu.edu.cn

Table of contents in Supporting Information:

1. Experimental Section

Materials: ammonium molybdate, thiourea, melamine and red phosphorus were purchased from Sinopharm Chemical Reagent. The Pt/C catalyst (20wt% Pt on Vulcan XC72R carbon) was purchased from Johnson Matthey Corporation. Other chemicals were purchased from Beijing Chemical Reagent Company. Tetrabutylammonium perchlorate and acetonitrile were purified to remove trace oxygen and water.

Synthesis of C_3N_4 template: The C_3N_4 template was synthesized by a one-step pyrolytic approach in air. Briefly, melamine with proper quantity was put into crucible. The crucible was heated to 550 ºC with a rate of 4 ºC min^{-1} in muffle furnace, maintained for 180 min, and then cooled to room temperature. The as-prepared C_3N_4 was yellow in colour, which was grinded into powder for further use.

Synthesis of the MoO_3/C_3N_4 intermediate: 4.0 g of C_3N_4 sacrificial template and 0.3 g of ammonium molybdate were mixed in mortar and grinded into homogeneous yellow powder. The resulting powder was transferred into crucible and heated to 300 in air with a rate of 3 ºC min^{-1} to obtain the yellowish-green intermediate of MoO_3/C_3N_4.

Synthesis of ultrathin P-MoS_2 nanosheets: 4.0 g of MoO_3/C_3N_4 intermediate, 2.0 g of thiourea and 0.2 g of red phosphorus were mixed by grinding, and then the resulting powder was transferred into the furnace. The furnace was heated to 600 ºC with a rate of 2.5 ºC min^{-1} under nitrogen and maintained for 240 min, followed by elevating to 800 ºC and maintaining for 180 min.

Synthesis of ultrathin MoS_2 nanosheets: The synthetic approach is similar to the ultrathin P-MoS_2 nanosheets without the addition of red phosphorus.

Physical characterization: The data of transmission electron microscopy (TEM) were recorded on TecnaiF20. The scanning electron microscopy (SEM) measurements were performed on a HITACHI SU8020 instrument. The X-ray powder diffraction (XRD) patterns were measured in reflection mode (Cu KR radiation) on shimadzu XRD-6000. X-ray Photoelectron Spectroscopy (XPS) spectra were recorded by using ESCALAB 250 spectrometer with a mono X-Ray source Al Kα excitation (1486.6 eV). Raman spectra were measured with a Horiba LabRAM HR Evolution spectrometer. Nitrogen sorption experiments were performed with a Quadrasorb at 77 K, and the samples were degassed at 150 °C for 20 h before measurements. The data were analyzed with Quantachrome software. The TGA was carried out on a TG 209 F1 Netzsch apparatus under nitrogen with a 10 °C min^{-1} heating rate.

Oxygen reduction reaction (ORR) measurements: The electrochemical tests were conducted using CHI 660B (shanghai, China) with a typical three-electrode cell. A platinum wire was used as the counter-electrode and a saturated calomel electrode (SCE) as the reference electrode. The working electrode was prepared by applying the catalyst ink onto a pre-polished glassy carbon electrode (GCE) and a GC rotating disk electrode (RDE). Briefly, the sample was dispersed in mixed solvent of ultrapure water and DMF (v/v=1:1) under ultrasonication for 15 min to form a uniform sample ink (2 mg mL^{-1}). A total of 10 μL well-dispersed sample ink was applied onto the clean surface of the electrode (3 mm in diameter). The loading for each MoS_2 sample as well as the commercial Pt/C catalyst was 283 μg cm^{-2}. Since the 20% Pt/C catalyst was used, the Pt content is calculated as 56.6 μg cm^{-2}. After drying at room temperature, 5 μL of Nafion solution in ethanol (0.5 wt%) was dropped onto the surface of the catalyst layer to form a thin

protective film. The addition of a small amount of Nafion could effectively improve the dispersion of the catalyst suspension and enhance its binding onto the GCE surface. The as-prepared electrodes were dried at room temperature for overnight. Prior to the experiments, the electrolyte solutions were purged with O_2 for 30 min. And the headspace of the electrochemical cell was continuously purged with O_2 during the measurements. All the experiments were conducted at ambient condition. The Koutechy-Levich (K-L) plots were analysed at different electrode potentials. Based on the K-L equation, the electron transfer number (n) is calculated from the slope of the K-L plot:

$$\frac{1}{J} = \frac{1}{J_k} + \frac{1}{B\omega^{1/2}} \quad (1)$$

$$B = 0.62nFC_0(D_0)^{2/3}(\upsilon)^{-1/6} \quad (2)$$

in which, J represents the measured current density, J_K is the kinetic limiting current density, ω is the electrode rotating rate, n is the electron transfer number, F is the Faraday constant (F = 96485 C mol^{-1}), C_0 is the bulk concentration of O_2 ($C_0 = 1.2\times10^{-6}$ mol cm^{-3}), D_0 is the diffusion coefficient of O_2 in 0.1 M KOH ($D_0 = 1.9\times10^{-5}$ cm^2 s^{-1}), and υ is the kinetic viscosity (υ = 0.01 cm^2 s^{-1}). All the potentials reported were referenced to a reversible hydrogen electrode (RHE) by adding a value of (0.2438+0.059 pH) V.

The measurement of frontier molecular orbital energy:[1] The electrochemical tests were conducted in acetonitrile containing 0.1 M tetrabutylammonium perchlorate using CHI 660B (shanghai, China) with a typical three-electrode cell. A platinum wire was used as the counter-electrode and a Ag/Ag^+ (0.01 M $AgNO_3$ in acetonitrile) electrode as the reference electrode. The working electrode was prepared by applying the catalyst ink onto a pre-polished glassy carbon electrode (GCE). The acetonitrile and tetrabutylammonium perchlorate were thoroughly purified by removing trace oxygen and water. Ferrocene was used as the reference to rectify the potential.

2. Detailed discussions on the substantial difference of the two works on P-MoS_2 ultrathin nanosheets and Oxygen edge-replaced MoS_2 ultrathin nanosheets.

Herein, to remove the possible misleading to authors, the substantial difference between these two works has been discussed. Actually, these two works are independent of each other, aiming at exploring novel synthetic approaches to chemically fabricate different type of heteroatoms to further modify the physical and chemical properties of MoS_2 ultrathin nanosheets. The substantial difference between them is emphasized as follows:

I. The heteroatom involved and its relative electronegativity, as well as the fabrication sites or domain are different in these two works. The work on P-doped MoS_2 nanosheets describes successful engineering low-electronegative heteroatom phosphorus into the basal plane of ultrathin MoS_2 nanostructure, while the other concerns controllable S-edge replacement by high-electronegative oxygen atom in the MoS_2 nanosheets.

II. To realize phosphorus or oxygen heteroatom engineering into the ultrathin MoS_2 nanostructure, different synthetic approaches are developed consequently. (i) A facile in-situ pyrolytical strategy is firstly explored and successfully chemical doping of P atom in the basal plane of MoS_2 ultrathin nanosheets is achieved. In principle, some other heteroatoms may also be similarly doped. However, the practical O atom doping by using the same synthetic strategy meets a great challenge, due to the difficulty in finding a suitable oxygen source, which should sustain in the reducing atmosphere at high temperature, since a large amount of NH_3 and HCN gases are released from decomposition of C_3N_4 tamplate during the initial pyrolytical process. Therefore, the developed in-situ pyrolytical approach is not available to doping of O atom in MoS_2 ultrathin nanosheets. Similar phenomenon can also be found in pyrolytical synthesis of heteroatom doped graphene. In literature, various heteroelements have been doped in graphene except for oxygen element. (ii) For realizing oxygen fabrication, a two-step strategy is subsequently developed in the second work: 1) pyrolytical synthesis of ultrathin MoS_2 nanosheets, 2) edge-incorporation of oxygen atom by a post-modification process in an aqueous solution of hydrogen peroxide, generating $Mo^{(IV)}$-O structure at the edges of MoS_2 ultrathin nanosheets.

III. The proposed ORR enhanced mechanism is diverse in the two works. Theoretical study has already suggested that the heteroatoms doping in the basal plane of MoS_2 nanosheets could integrally modulate the electronic structure and frontier orbital energy and bring additional active sites for catalysis. In the work on basal plane doing of P atom, the raise of frontier orbital energy to the MoS_2 nanosheets has been proved by performing electrochemical characterizations. Meanwhile, previous theoretical study suggests that doping of low-electronegative atom in the basal plane may also bring an abundance of active sites. Hence, the enhanced ORR mechanism of P-MoS_2 catalyst is mainly ascribed to the extra catalytic sites generated upon in-plane P atom doping as well as the facile electron transport originated from the raised frontier orbital energy. In the work of O-edge fabrication, the high-electronegative O atom may be prone to polarize the adjacent Mo edges in nanosheets, leading to more positive charges that preferentially adsorb oxygen molecule. Moreover, the formation of terminal $Mo^{(IV)}$-O structure could partially change the electronic structure at the MoS_2 nanosheets edge, leading to decrease of the band-gap and enhancement of intrinsic conductivity of the material, which has been indicated by Y. Xie et.al in a previous theoretical study. Therefore, preferential adsorption of oxygen molecule via polarizing adjacent Mo edges by high-electronegative O atom as well as partially enhanced conductivity may be responsible for efficient ORR.

In conclusion, despite both works focus on heteroatoms engineering in MoS_2 nanosheets for enhanced ORR by modulating the electronic property of these nanosheets, they are diverse with a lot of differences, including the heteroatom involved and its relative electronegativity, the fabrication sites or domain, the synthetic approaches developed, as well as the enhanced ORR catalytic mechanism proposed.

3. **Figure S1.** Photograph of ultrathin P-MoS_2 nanosheets.

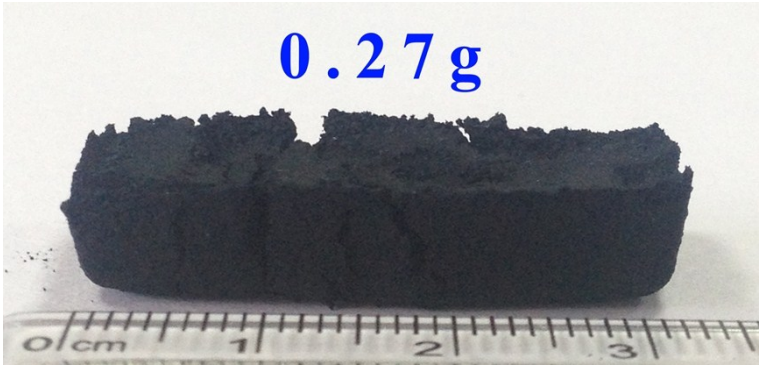

4. **Figure S2.** TGA curve of the precursors for ultrathin P-MoS_2 nanosheets measured from 25 to 800°C in nitrogen atmosphere with a heating rate of 10°C min^{-1}.

The thermogravimetric analysis (TGA) on the precursors (MoO_3/g-C_3N_4 intermediate, sulfourea and red phosphorus) manifests a two-step approach for pyrolytic synthesis of P-MoS_2. In the first process, sulfourea gradually decomposed in quartz tube under 300 °C to form a circumstance of H_2S gas. With subsequent increase of temperature, the layered MoO_3 in the intermediate was transformed into ultrathin MoS_2 nanosheets. Meanwhile, phosphorus, as the form of gas, invaded into the low-crystallized MoS_2 nanosheets to realize heteroatoms doping. The second-step pyrolysis took place in the temperature range of 550-700 °C. With the increase of temperature, decomposition of the g-C_3N_4 template accompanied by gradual crystallization of ultrathin P-MoS_2 nanosheets led to a 64% weight loss in TGA. At higher temperature, the template is completely decomposed with a large amount of gas released. During which, the lamellar structure of ultrathin P-MoS_2 nanosheets randomly curved, leading to a 3D porous structure.

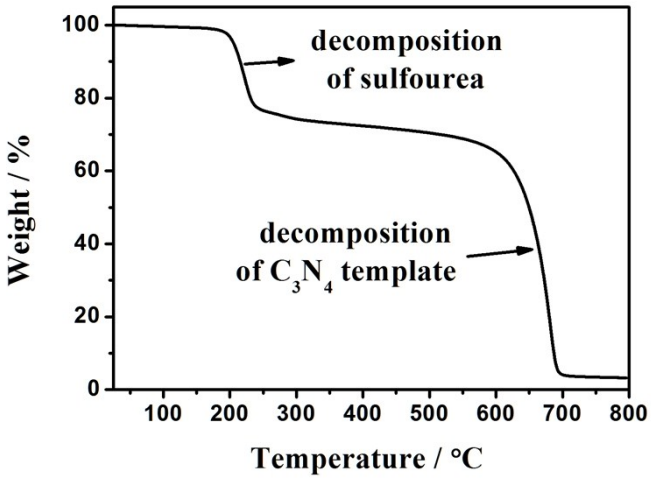

5. **Figure S3.** SEM and TEM images of the C_3N_4 template.

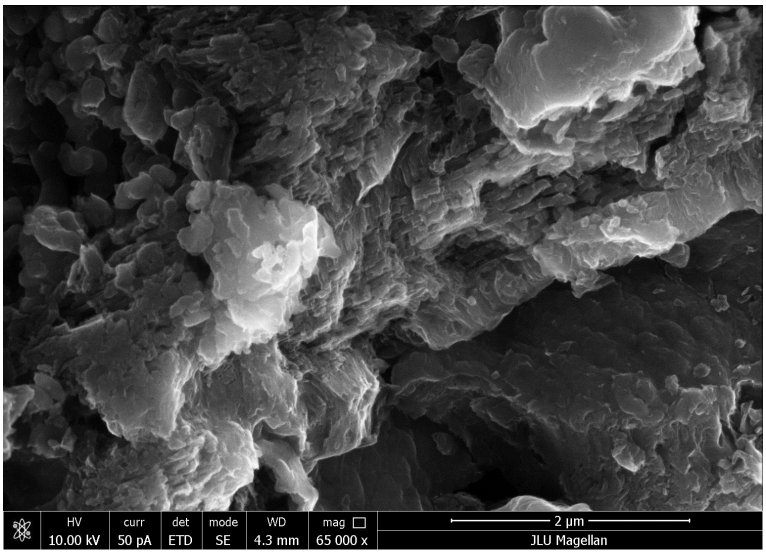

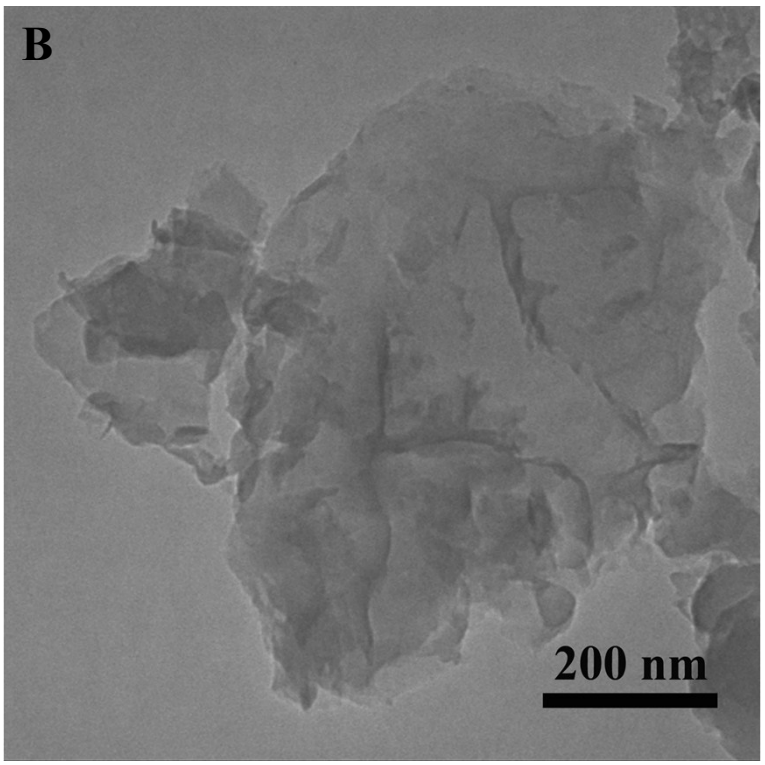

6. **Figure S4.** SEM image of the ultrathin P-MoS_2 nanosheets.

A

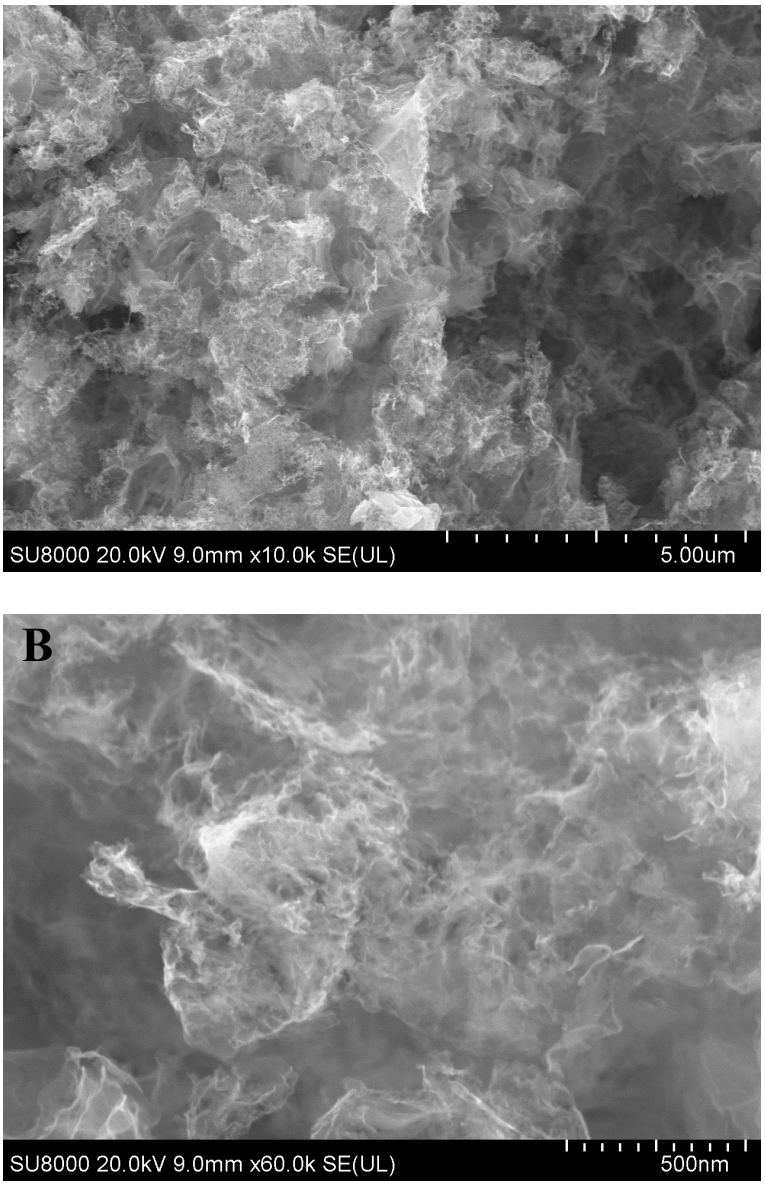

7. **Figure S5.** SEM image of pristine MoS_2 ultrathin nanosheets.

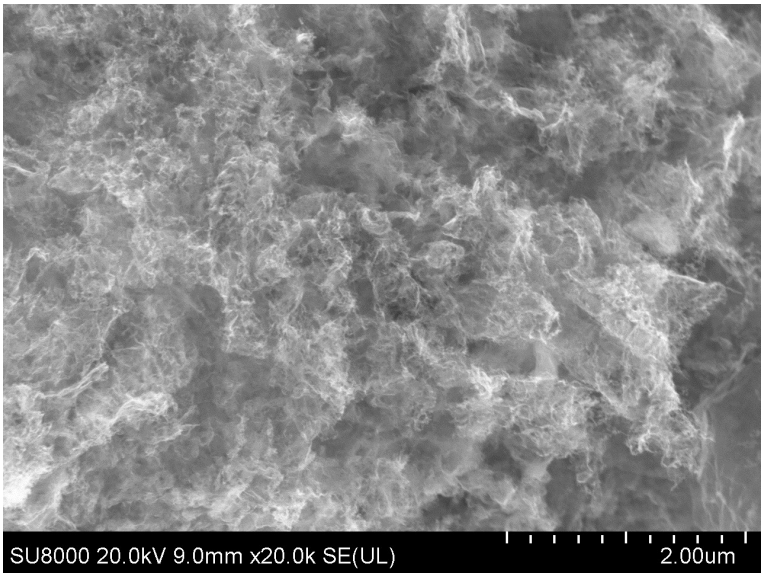

8. **Figure S6.** TEM images of ultrathin P-MoS_2 nanosheets.

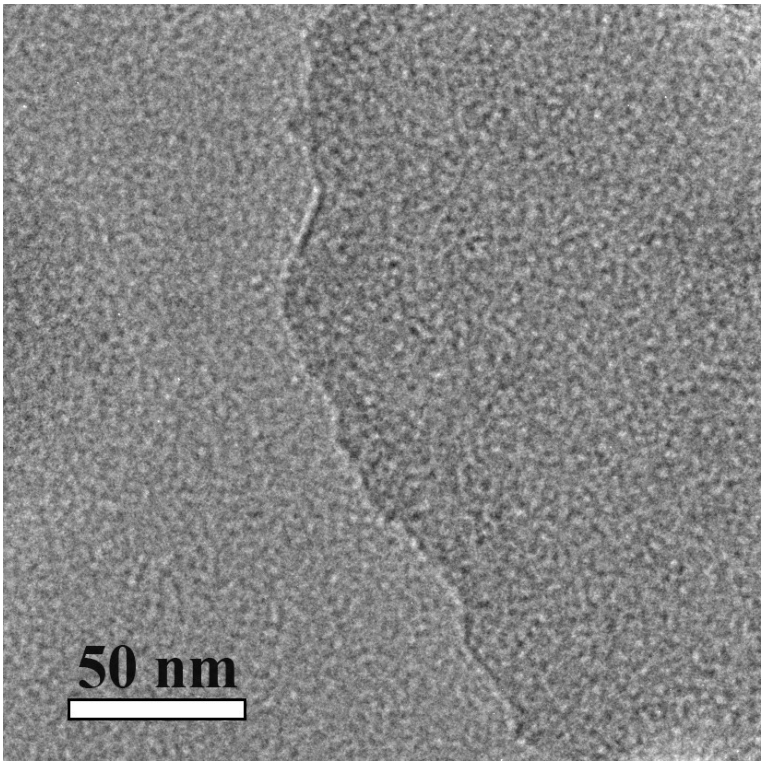

9. **Figure S7.** Raman spectra of ultrathin P-MoS_2, pristine MoS_2 and bulk MoS_2.

The Raman spectrum of P-MoS_2 in the informative range from 360 to 450 cm^{-1} reveals the characteristic peaks of MoS_2. The two dominant peaks of the hexagonal MoS_2,[2] in-plane E^1_{2g} and out-of-plane A^1_g vibrational modes, appear at 384 and 403 cm^{-1} respectively. Previous work has revealed that with decreasing number of the MoS_2 layers, the frequency difference between E^1_{2g} and A^1_g Raman peak decreases stepwisely.[3] The frequency difference of P-MoS_2 is 19 cm^{-1}, which is much smaller than the pristine MoS_2. This result indicats that the nanosheets of P-MoS_2 are ultrathin, constituted of mainly few layers. Meanwhile, the relatively broad and weak peak of E^1_{2g} indicates that the crystal structure of ultrathin P-MoS_2 nanosheets is not perfect and the in-layer disorder or defects should exist,[4] originated from P-heteroatoms invading into the MoS_2 crystal structure.

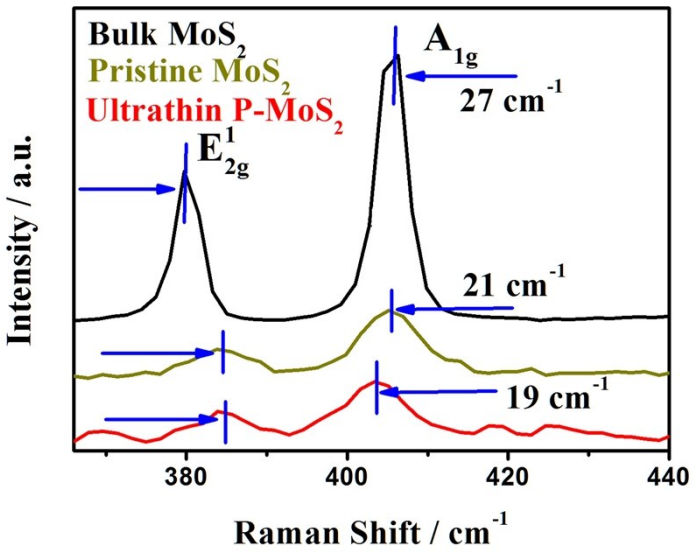

10. Figure S8. Nitrogen sorption measurements for ultrathin P-MoS_2 nanosheets.

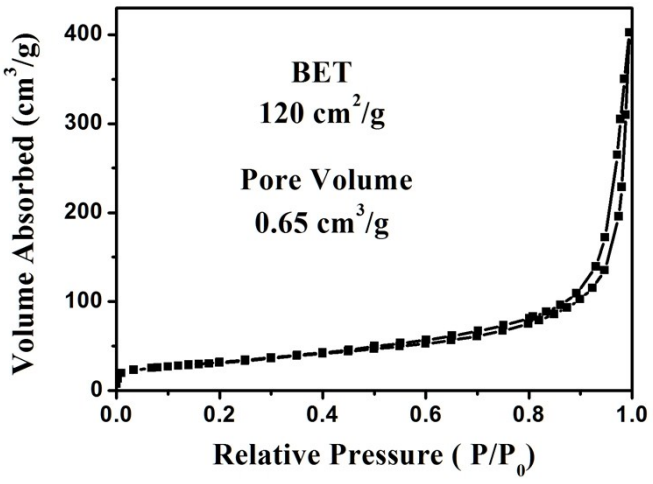

11. Figure S9. Electrochemical impedance spectra (EIS) of P-MoS_2, MoS_2 and Pt/C catalysts.

The spectra of electrochemical impedance reveals that the MoS_2 catalysts exhibit very similar EIS behavior, indicating that P-doping in the nanosheet plane only brings minor change of the conductivity of these 2D MoS_2 nanocatalysts. Compared to the Pt/C catalyst, the conductivity of the MoS_2-based catalysts is improved.

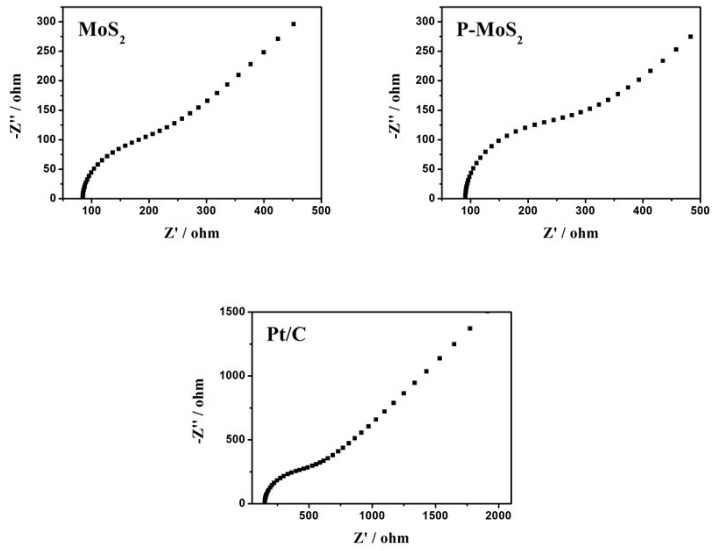

12. Figure S10. CVs of various MoS_2 samples and commercial Pt/C catalyst in N_2- (black) and O_2- (red) saturated electrolyte.

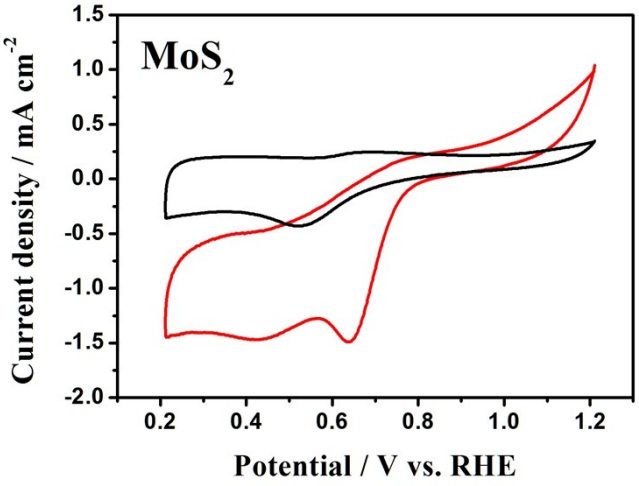
MoS2
Current density / mA cm-2
Potential / V vs. RHE
1.5
1.0
0.5
0.0
-0.5
-1.0
-1.5
-2.0
0.2
0.4
0.6
0.8
1.0
1.2

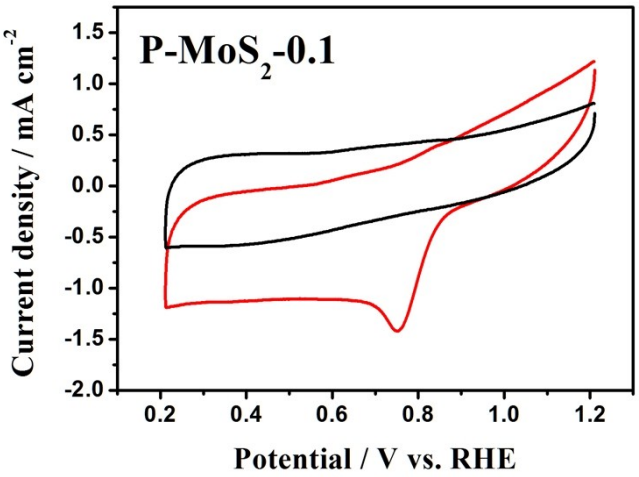
P-MoS2-0.1
Current density / mA cm-2
Potential / V vs. RHE
1.5
1.0
0.5
0.0
-0.5
-1.0
-1.5
-2.0
0.2
0.4
0.6
0.8
1.0
1.2

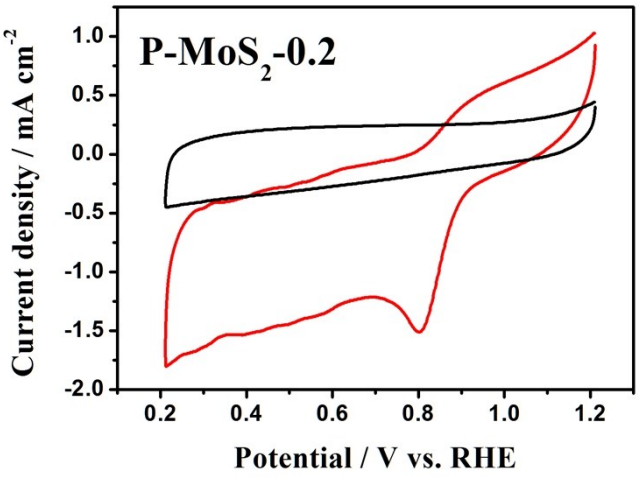
P-MoS2-0.2
Current density / mA cm-2
Potential / V vs. RHE
1.0
0.5
0.0
-0.5
-1.0
-1.5
-2.0
0.2
0.4
0.6
0.8
1.0
1.2

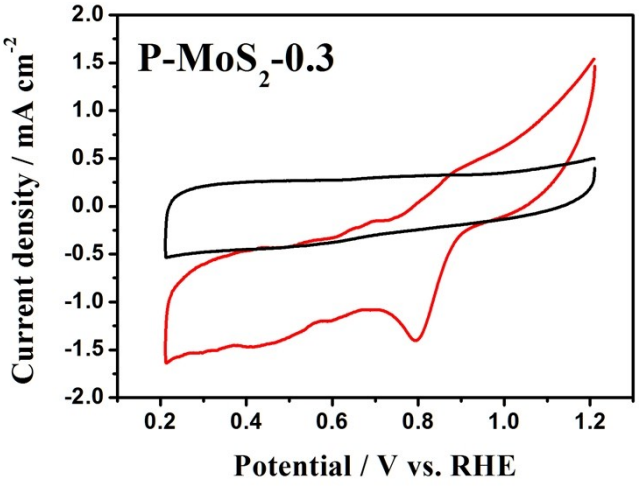
P-MoS2-0.3
Current density / mA cm-2
Potential / V vs. RHE
2.0
1.5
1.0
0.5
0.0
-0.5
-1.0
-1.5
-2.0
0.2
0.4
0.6
0.8
1.0
1.2

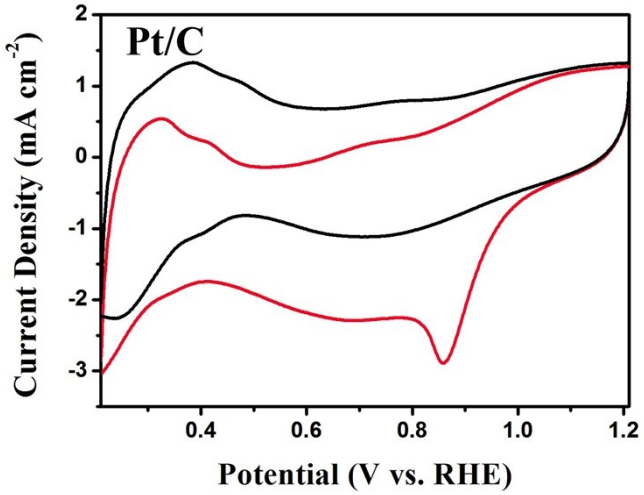
Pt/C
Current Density (mA cm-2)
Potential (V vs. RHE)
2
1
0
-1
-2
-3
0.4
0.6
0.8
1.0
1.2

13. Figure S11. (a) RDE LSVs and (b) Koutecky–Levich plots of ultrathin MoS_2 nanosheets in O_2-saturated 0.1 M KOH.

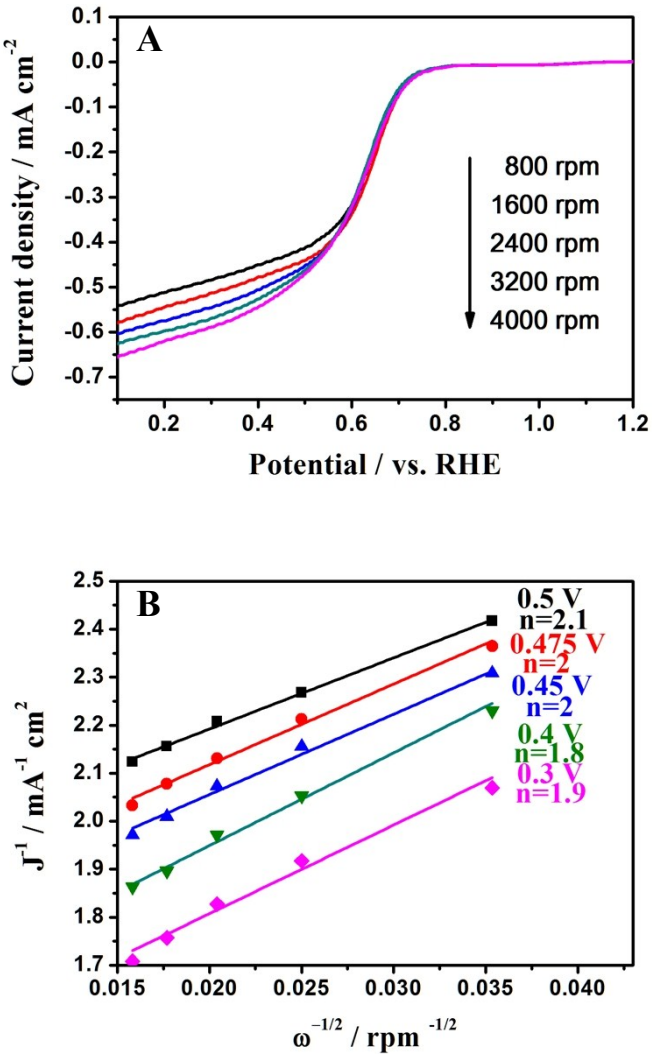

14. Figure S12. (a) RDE LSVs and (b) Koutecky–Levich plots of 20% Pt/C catalyst in O_2-saturated 0.1 M KOH.

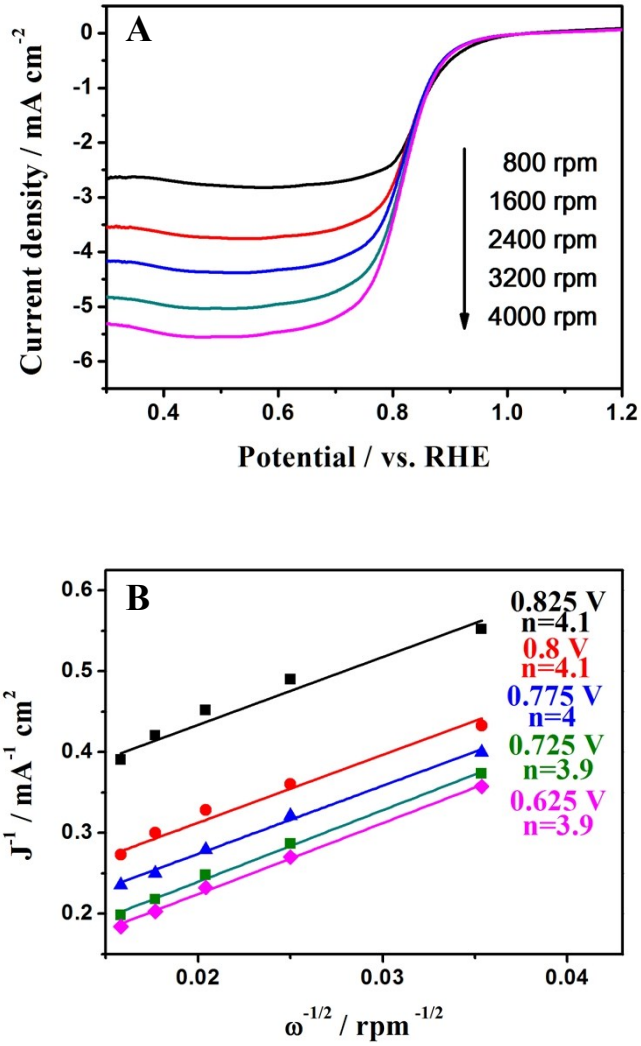

15. Figure S13. Schematic diagram of P-MoS_2 ORR catalytic process.

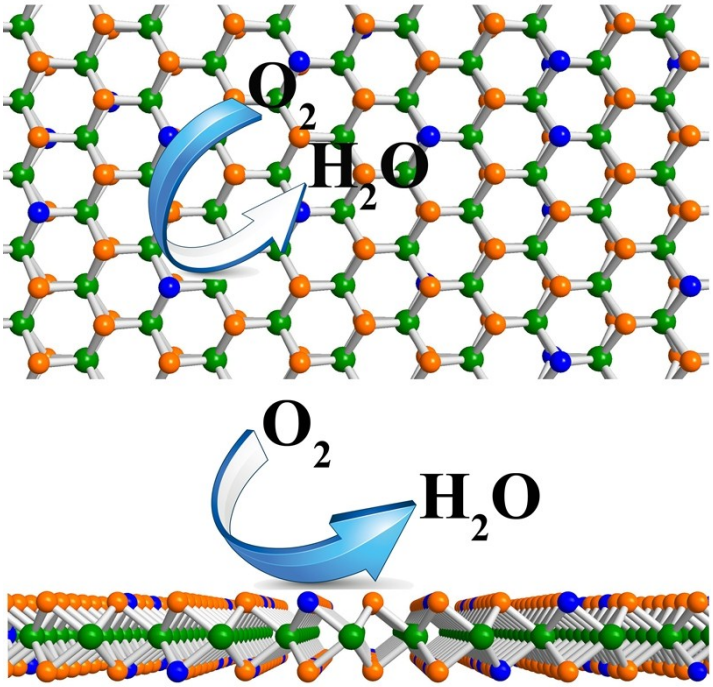

16. Figure S14. Durability of P-MoS_2 and 20% Pt/C catalysts in O_2-saturated 0.1 M KOH.

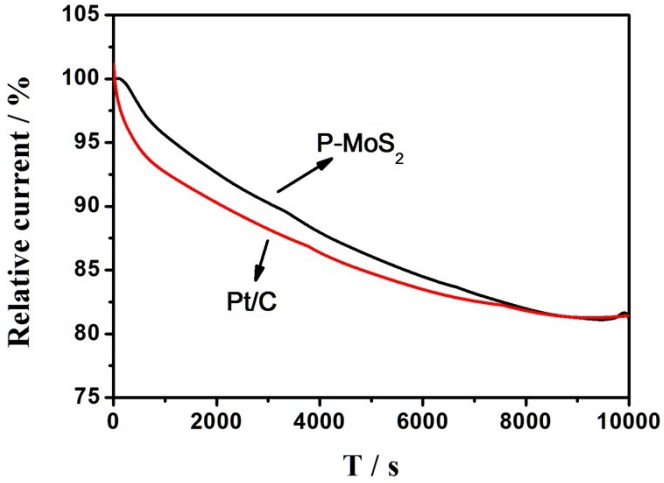

17. Table S1. The frontier molecular orbital energies of P-MoS_2 nanosheets and MoS_2 nanosheets.

	HOMO	LOMO
P-MoS_2 nanosheets	-6.37 eV	-4.21 eV
MoS_2 nanosheets	-6.39 eV	-4.50 eV

18. References

[1] W. B. Song, X. Chen, F. Wu, W. J. Tian, Y. G. Ma, H. D. Xu, *Chemical Journal of Chinese Unviersites* 2000, **9**, 1422.

[2] Y. Yan, B. Y. Xia, X. M. Ge, Z. L. Liu, J. Y. Wang, X. Wang, *Acs Appl. Mater. Inter.* 2013, **5**, 12794.

[3] Q. Q. Ji, Y. F. Zhang, T. Gao, Y. Zhang, D. L. Ma, M. X. Liu, Y. B. Chen, X. F. Qiao, P. H. Tan, M. Kan, J. Feng, Q. Sun, Z. F. Liu, *Nano Lett.* 2013, **13**, 3870.

[4] D. S. Kong, H. T. Wang, J. J. Cha, M. Pasta, K. J. Koski, J. Yao, Y. Cui, *Nano Lett.* 2013, **13**, 1341.